Astron. Astrophys. 228, 284–294 (1990)

ASTRONOMY AND ASTROPHYSICS

Nonlinear dynamos with magnetic buoyancy in spherical geometry

D. Moss*, I. Tuominen, and A. Brandenburg

Observatory and Astrophysics Laboratory, University of Helsinki, Tähtitorninmäki, SF-00130 Helsinki 13, Finland

Received May 22, accepted May 30, 1989

Abstract. We compute numerical solutions for axisymmetric mean field dynamos of α^2 and $\alpha^2\omega$ type in spherical geometry. In particular we study the effects of including a term in the magnetohydrodynamic equations which represents the upward advection of fields by magnetic buoyancy. For the buoyancy limited α^2 dynamo we find that, for certain parameter values, this model may have two stable solutions, of opposite parity properties with respect to the equator. In our $\alpha^2\omega$ dynamo models for smaller values of a dynamo number, odd parity solutions are stable, but for larger values it is the even parity solutions that are stable. These results concerning the stability of pure parity solutions are similar to those found in an earlier study in which the nonlinearity was a simple α-quenching.

The effects of buoyancy on the periods of our $\alpha^2\omega$ dynamos is small: increasing the buoyancy parameter slightly decreases cycle periods. In contrast to the α-quenched $\alpha^2\omega$ models studied previously, we do not find any finite parameter range in which stable mixed parity solutions are present in purely buoyancy-limited models. In particular, 'torus-type' solutions of the type discovered previously in α-quenched dynamos are not found.

We also present some models with both buoyancy and α-quenching included. The most noticeable effect of adding a buoyancy term to the α-quenched solutions is that the amplitude of the finite amplitude parity oscillations (tori and limit cycles) previously found is reduced.

Key words: dynamos: nonlinear – buoyancy – magnetohydrodynamics – solar cycle

1. Introduction

The magnetic fields of the sun, solar type stars and the planets are widely (but not universally) believed to be the result of dynamo action in a rotating, electrically conducting fluid. Mean field dynamo theory seems capable of explaining many of the features observed on the sun (e.g. Brandenburg and Tuominen, 1988), but it is clear that very simple kinematic models, of the kind developed by Steenbeck and Krause (1969), although explaining successfully the basic mechanism of the magnetic oscillations, are inadequate to explain quantitatively many features of the solar cycle or analogous cycles in active stars with convective envelopes.

The magnetic field strength in the sun, other stars or planets is believed to be limited in magnitude by nonlinear effects. For example, the field can inhibit convection and so reduce the "α-effect". The differential rotation can be reduced by the Lorentz force of the dynamo field. Magnetic buoyancy may rapidly remove flux from the convection zone. The latter effect has been widely studied in recent years (e.g. Parker, 1979). Van Ballegooijen (1982) discussed the magnetic flux storage problem, important because the rise times of buoyant magnetic flux tubes may be much shorter than the solar cycle period (e.g. Moreno-Insertis, 1983). Besides the gross effects of buoyancy on field generation and limitation, the stability properties of buoyancy-limited dynamos are of importance, in particular because we expect that it is the stable solutions that are realized in practice. The stability problem was recently discussed by Krause and Meinel (1988).

In previous papers of this series (Brandenburg et al., 1989a: Paper I; Brandenburg et al., 1989b, Paper II) we have described a program which performs nonlinear calculations for a simple fluid dynamo model. Whilst the solutions are limited in that the fluid is assumed to be incompressible and there is a strict requirement of axisymmetry, they do provide a considerable advance on most previous nonlinear dynamo calculations in that calculations are performed on a two-dimensional r, θ grid (spherical polar coordinates), in contrast to the severe truncation to 0(10) dependent variables often employed in previous (one-dimensional) studies. A particular feature of our numerical scheme is that we calculate explicitly on the range $(0, \pi)$, thus avoiding prescribing the parity of our solutions by means of boundary conditions imposed on $\theta = \pi/2$. This has already produced several interesting new results.

Of course there is a price for this advance in that considerably increased computational resources are needed. However in Papers I and II we were able to investigate some interesting phenomena concerning the nonlinear limitation of mean field dynamos by the action of the Lorentz force on the mean motions and also by a simple "α-quenching" mechanism. Whilst our solutions did not show the richness in terms of bifurcations and transitions to chaos of some of the "toy" systems previously investigated that are of interest in the study of general nonlinear dynamical systems (e.g. Lorenz, 1963; Ruzmaikin, 1981; Jones et al., 1983), they do have a much closer and more readily apparent relation to "real" geo- and astrophysical dynamos such as are believed to operate in the earth, sun and lower main sequence stars.

Send offprint requests to: David Moss

* Permanent address: Mathematics Department, The University, Manchester M13 9PL, UK

As mentioned above, in addition to the back-reaction on the mean motions and the reduction of the magnitude of the α effect from the interaction of the dynamo generated field with the small scale turbulence, at least one other mechanism seems likely to be important in limiting the growth of mean field astrophysical dynamos, namely magnetic buoyancy. Indeed, Noyes et al. (1984) have argued that this must be the dominant mechanism. Whilst the importance of this effect in the solar convection zone has been disputed, as a number of mechanisms may act to mitigate its action, it seems clear that a thorough understanding of nonlinear dynamos must include a study of its effects. Thus in this paper we include a simple parameterization of magnetic buoyancy in the dynamo model described in Papers I and II. The initial investigation is limited to the case where buoyancy is the only nonlinear effect active. Later we include α-quenching also. As in the previous papers we solve the dynamo equations in a complete sphere. Even with our grossly simplified model there are several free parameters, and the regions of parameter space investigated are necessarily rather subjectively chosen and limited. Thus we can make no claim to completeness, but rather just attempt to display some of the phenomena that we encountered.

2. The model

2.1. A simple representation of the effects of buoyancy

The simplest order of magnitude argument to estimate the modification of the standard dynamo equation of mean field electrodynamics is to say that, since the Lorentz force is quadratic in $\mathbf{B}$, then the magnitude of the buoyant velocity is proportional to $\mathbf{B}^2$. Thus a term

$$\mathbf{u}_B = \xi \mathbf{B}^2 \hat{\mathbf{r}}, \tag{1}$$

ζ = positive constant, is added to the mean velocity appearing in the mean field dynamo equation, which then takes the form

$$\partial \mathbf{B}/\partial t = \nabla \times (\mathbf{u} \times \mathbf{B} + \mathbf{u}_B \times \mathbf{B} + \alpha \mathbf{B}) - \nabla \times (\eta \nabla \times \mathbf{B}), \tag{2}$$

where $\mathbf{u}$ is the large scale velocity field, α is the usual (isotropic) helicity parameter and η is the diffusion coefficient.

A superficially similar expression for the advection of field radially outwards can be derived by the following argument, due to Rädler (private communication).

Consider a system of rising and falling motions, such as are present in a convection zone even in the absence of magnetic fields. Let subscripts u and d denote "up" and "down" motions respectively. Suppose that the areas occupied by up and down motions are S_u and S_d. Then mass conservation gives

$$\rho_u u_u S_u = \rho_d u_d S_d,$$

where u_u and u_d are positive velocities. Then the mean radial velocity is

$$\langle u_r \rangle = (u_u S_u - u_d S_d)/(S_u + S_d).$$

Put

$$\rho_u = \rho_d - \Delta\rho, \quad \Delta\rho > 0.$$

Then

$$\langle u_r \rangle = S_u/(S_u + S_d) u_u \Delta\rho/\rho$$
$$= k(\Delta\rho/\rho) u_u, \quad \text{where} \quad k \sim 1/2.$$

In a compressible gas without a magnetic field horizontal pressure balance gives a relation between pressure and temperature. In the presence of magnetic field the condition of horizontal pressure balance will give $\mathbf{B}^2/2\mu$ to be of the same order of magnitude as $\Delta\rho$ (essentially approximate equipartition of energies).

If

$$\Delta p = -c^2 \Delta\rho,$$

c the speed of sound, we get

$$\Delta\rho/\rho \sim v_A^2/c^2,$$

where v_A is the Alfvén velocity. Thus

$$\langle u_r \rangle \sim 0.5 k v_A^2/c^2 u_u,$$

and

$$\mathbf{u}_B = \zeta' \mathbf{B}^2 \hat{\mathbf{r}}.$$

where $\xi' \simeq k u_u/(2\mu\rho) > 0$.

This is of the same form as expression (1), but the mechanism is more akin to a "mean field pumping". It seems probable that $\xi' < \xi$ in many cases of interest. We shall adopt Eq. (1) without further discussion of the underlying mechanism. In this paper we are only concerned with the general effects of buoyancy and we are not attempting to produce a detailed model of any astrophysical system. Thus we shall assume ξ to be independent of position and time. The magnitude of ξ can only be estimated from a much more complete theory than ours, and so we shall treat ξ on an arbitrary (positive) constant. It is probable that ξ would vary significantly through a convective envelope. (When buoyancy is the only nonlinear process acting then explicit occurrence of a constant ξ can be removed by scaling, see below).

Taking the radius of the sphere, R, as the unit of length and scaling with unit of time R^2/η, Eq. (2) can be written in dimensionless form as

$$\partial \mathbf{B}/\partial t = \nabla \times (\mathbf{u} \times \mathbf{B} + \alpha \mathbf{B} + \Gamma \hat{\mathbf{r}} \times \mathbf{B}) - \nabla \times (\nabla \times \mathbf{B}) \tag{3}$$

where $\Gamma = \gamma \mathbf{B}^2$, $\gamma = \xi R/\eta$, and η is assumed to be uniform. Our large scale velocity u is taken to be a differential rotation, $\Omega x \sin\theta \hat{\phi}$, only ($x = r/R$). We use

$$\alpha = C_\alpha f(\mathbf{B}^2) \cos\theta. \tag{4}$$

We can define the two usual dimensionless parameters

$$C_\alpha = \alpha_0 R/\eta, \quad C_\omega = \Omega_0' R^2/\eta,$$

where Ω_0' is the radial derivative of the angular velocity, which is assumed to be constant in our models. When $f(\mathbf{B}^2) = 1$ (no nonlinear feedback onto the α-effect) then C_α, C_ω and Γ define the problem. Note that Eq. (3) then allows the scaling

$\mathbf{B} \to g\mathbf{B}^*$, $\gamma \to g^{-2}\gamma^*$, giving

$$\partial \mathbf{B}^*/\partial t = \nabla \times (\mathbf{u} \times \mathbf{B}^* + \alpha \mathbf{B}^* + \gamma^* \mathbf{B}^{*2} \hat{\mathbf{r}} \times \mathbf{B}^*) - \nabla \times (\nabla \times \mathbf{B}^*), \tag{5}$$

Thus the equation can be scaled to remove γ as a free parameter. Note further, however, that identical results for any given calculation will be obtained by solving Eq. (3) with different values of γ only if the initial field $\mathbf{B}(x, \theta, 0)$ of (3) is replaced by $\mathbf{B}^*(\mathbf{x}, \theta, 0) = g^{-1}\mathbf{B}(x, \theta, 0)$ in (5). In some instances the final solution seems to be independent of the form and magnitude of the initial field. In other cases this is not so. We adopted the computational procedure of starting our calculations with a standard set of

fields of given energy (see Sect. 3), and allowing γ to vary. This is equivalent to varying the initial energy at fixed γ. (This scaling was verified numerically.)

For some of our calculations we introduced a simple α-quenching, as in Paper I and II. We wrote

$$\alpha=\alpha_0/(1+\mathbf{B}^2/(2E_s)) \tag{6}$$

in (2). The physical motivation is that the helicity is reduced when the magnetic field becomes strong enough to affect the small scale dynamics – a simple model might take E_s to be the kinetic energy of the turbulence. (Note that $\mathbf{B}^2/2$ is the local magnetic energy density.) In dimensionless form (6) then becomes

$$f(\mathbf{B}^2)=(1+\alpha_B\mathbf{B}^2)^{-1}. \tag{7}$$

In Papers I and II, in the cases where this was the only nonlinear mechanism operating, we were able to scale so that $\alpha_B=1$ (cf. the above discussion). This is no longer possible when γ depends on $\mathbf{B}$. Then we must retain α_B as an additional parameter.

Finally, note that we retain the "α terms" in both the poloidal and toroidal induction equations even when $C_\omega\neq 0$ and so refer to $\alpha^2\omega$ dynamos.

2.2. *Other formulations*

Plausible arguments can be given for other simple representations of the effects of buoyancy. For example, a crude estimate of the rise rate of a buoyant flux *tube* might give $|\mathbf{u}_B|\propto v_A$ (e.g. Parker, 1979, Eq. (8.60)). Then Eq. (1) becomes

$$\mathbf{u}_B=\xi_1|\mathbf{B}|\hat{\mathbf{r}} \tag{8}$$

Now, of course, the scaling is $\gamma\to g^{-1}\gamma^*$, cf. Eq. (5). We briefly investigate the effects of such a choice in Sect. 4.4.

Further, Eq. (1) gives a radial component of velocity which does not vanish at $r=R$ since only the toroidal field is constrained to be zero there. It would be relatively straightforward to modify Eq. (1) so that $\mathbf{u}_B\to 0$ smoothly as $r\to R$ by introducing a suitable function of radius multiplying ξ. An even more straightforward procedure is to replace $\mathbf{B}$ by the toroidal part of the field, $\mathbf{B}_T$, in (1) or (8) since $\mathbf{B}_T=0$ on $r=R$. However such changes will make significant changes in, at most, the α^2 models investigated (i.e. when $C_\omega=0$), since in the $\alpha^2\omega$ models the ratio of poloidal to toroidal field strength is small, except very near $r=R$. In Sect. 4.5 we test the sensitivity of our models to such a change.

3. Numerical procedures

The numerical scheme to solve Eq. (3) was described in Paper I. We implemented it on a $NI\times NJ$ grid, covering the range $0\leqslant x\leqslant 1$, $0\leqslant\theta\leqslant\pi$. For many of the computations described we took $NI=21$, $NJ=41$. Typically the time step, $\Delta\tau$, was in the range 2×10^{-4} to 5×10^{-5}. We tested the accuracy of our results in a number of instances by rerunning the calculations with $NI=41$, $NJ=81$ and $\Delta\tau=2-5\times10^{-5}$. In general the agreement was very good and, except where an explicit comment to the contrary is made, we feel that the results obtained on the standard grid would not be significantly altered by using higher resolution.

We constructed a standard set of initial fields by taking linear combinations of odd (A) and even (S) eigenfunctions of the spherical α^2 dynamo, with $\alpha\propto\cos\theta$. These combinations can be described by the "parity parameter" P (Paper I),

$$P=(E^{(S)}-E^{(A)})/(E^{(S)}+E^{(A)}), \tag{9}$$

where $E^{(S)}$ and $E^{(A)}$ are, respectively, the energies in the parts of the field symmetric and antisymmetric with respect to the plane $\theta=\pi/2$. Thus $-1\leqslant P\leqslant 1$. $P(\tau)$ is also useful in describing and classifying the evolution of the models.

4. Results

4.1. *α^2 dynamos with buoyancy*

The critical dynamo numbers for the "standard" α distribution (Sect. 2) when $C_\omega=0$ are $C_\alpha^{(A)}=7.64$, $C_\alpha^{(S)}=7.81$, the superscripts (A) and (S) denoting fields of strictly odd ("dipolar") and even ("quadrupolar") parity respectively (cf. Roberts, 1972). With our standard 21×41 grid we obtained values of 7.62 and 7.79 respectively. The poloidal field lines and toroidal field contours are shown in Fig. 1. Both bifurcations are supercritical.

We then took a clearly supercritical value, $C_\alpha=10.0$, and investigated how varying the initial field configuration affected the final state. Initial fields were constructed as described in Sect. 3. In Fig. 2 the run of the parity parameter, $P(\tau)$, is shown for a number of such calculations with $-0.9\leqslant P(0)\leqslant 0.9$. (In the absence of numerical noise, cf. the similar discussion in Paper I, solutions with $P(0)=\pm1$ will retain their original parity.) In each case the dynamo saturates and a steady state with constant energy is reached, but the final configuration depends on the initial parity value, with the "watershed" value of $P(0)$ being between 0.1 and 0.0. The final field configurations with $P\to\pm1$ are shown in Fig. 3. The concentration of the field towards the surface compared with Fig. 1 is apparent.

Very similar behaviour was found when $C_\alpha=15.0$ – in particular the watershed was still between $P(0)=0.0$ and 0.1, but the approach to the final state was much more rapid, even when $P(0)=0.0$. For all the α^2 dynamos investigated the final steady solution was independent of the value of γ, except for the normalization of the field discussed in Sect. 2.1.

4.2. *$\alpha^2\omega$ dynamo with buoyancy*

4.2.1. Influence of $P(0)$ on final state

For our study of $\alpha^2\omega$ dynamos we only used a linear differential rotation profile with $C_\omega=-10^4$. With our standard resolution we found the critical values of $C_\alpha^{(A)}$ and $C_\alpha^{(S)}$ to be, respectively, 0.55 and 0.72, which are again satisfactorily close to those of Roberts (1972). These bifurcations from the trivial solution are both supercritical and the corresponding critical solutions are limit cycles, at constant parity $P=\pm1.0$. At $C_\alpha=2.0$ we again investigated the influence of the initial parity, $P(0)$, of the field on the subsequent evolution. Illustrative results ($\gamma=0.01$) are displayed in Fig. 4a – it can be deduced that the final state is $P=+1$ except when the initial field is of pure A-type ($P(0)=-1.0$), but that the rate of evolution to this state varies quite sharply with $P(0)$. In Fig. 4c we show the field contours for a mixed parity configuration. A property of these solutions is that the energy (predominantly in the toroidal field) oscillates with constant amplitude as the parity changes (after a short initial relaxation), and that this period and amplitude are the same for the different $P(0)$. Figure 4b shows the variation of E for the case $P(0)=-0.9$, as P changes from -0.9 to 0.0.

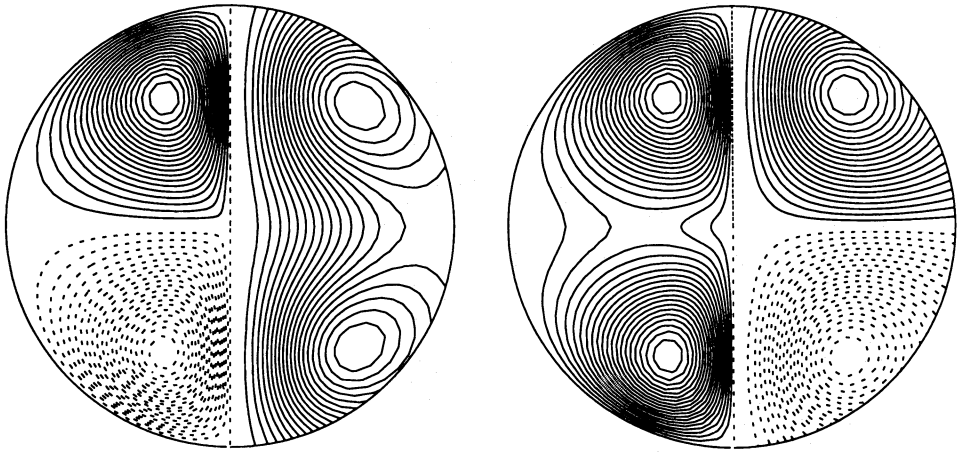

Fig. 1. Field contours for dipole and quadrupole eigenmodes, $C_\omega = 0.0$. Toroidal field contours in left hand half of each sphere, poloidal stream lines in right hand half

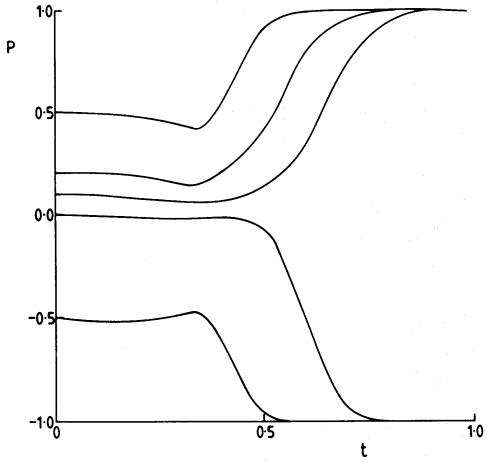

Fig. 2. $P(t)$ for various $P(0)$ with $C_\alpha = 10.0$, $C_\omega = 0.0$, $\gamma = 0.001$

In view of the results to be discussed in Sect. 4.2.3, we repeated these calculations with $C_\alpha = 1.0$. Now the final state was $P \simeq = -1.0$ for all $P(0)$ in the range investigated (-0.99, 1.0). The solutions seemed to be approaching $P = -1.0$ asymptotically but $P(\tau)$ continued to oscillate with very small amplitude in all the calculations that were continued to $\tau \gg 1$, and it was felt to be too expensive in computer time to run these calculations for long enough to see whether the oscillations eventually disappeared. Possibly the long-term behaviour is similar to that of the $C_\alpha = 1.10$, $\gamma = 1.0$ case discussed in Sect. 4.2.3. The time to evolve to $P \simeq -1.0$ depended very strongly on $P(0)$. For example, the solution with $P(0) = -0.9$ attained $P(\tau) \leqslant -0.97$ before $\tau = 0.1$, whereas when $P(0) = 0.0$, $\tau \approx 3.0$ is necessary before $P < -0.9$. The corresponding time at $P(0) = 0.2$ is about 8.0 and at $P(0) = 0.4$ a time $\tau > 20$ is estimated. When $P(0) = 0.99$, P initially increases to ~ 0.9998 but then declines slowly so that a time $\tau = 13$ is necessary for P to become less than 0.99, but by then the trend to smaller P values is clearly of similar form to those for smaller $P(0)$. Even in this case the variation of energy with time is unchanging after an initial relaxation which happens before $\tau \simeq 0.3$.

4.2.2. Effects of changing γ

Rerunning the $C_\alpha = 2.0$ calculations described above with $P(0) = 0.0$ and $\gamma = 1.0$ (with the same initial field energy, see discussion in Sect. 2) produced the $P(\tau)$ and $E(\tau)$ dependences shown in Fig. 5. The new feature here is the alternating large and small maxima and minima in E and the doubly periodic variation of P. By time $\tau = 1.5$, $P \approx 1$, although the oscillations, much reduced in

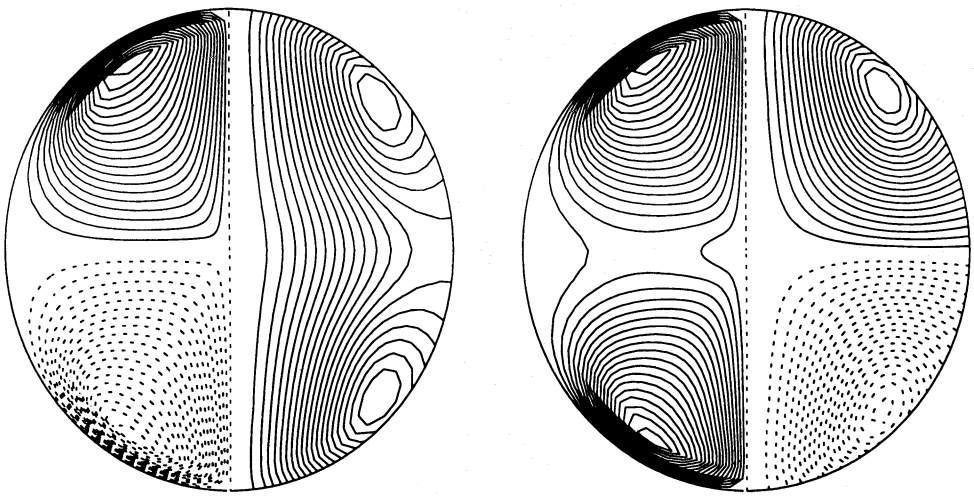

Fig. 3. Field contours for $P = \pm 1$, $C_\alpha = 10.0$, $C_\omega = 0.0$, $\gamma = 0.001$. Toroidal field contours in left hand half-sphere, poloidal field lines on right

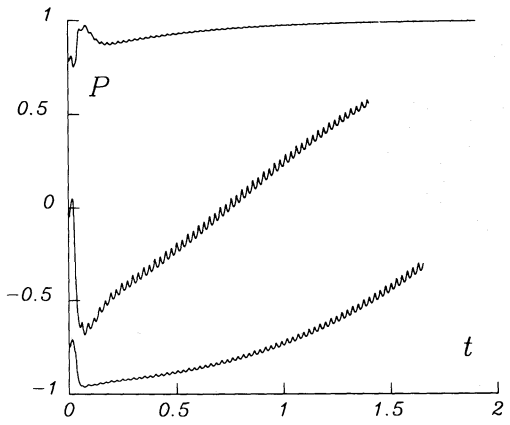

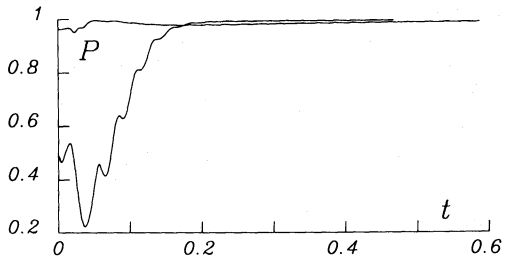

a

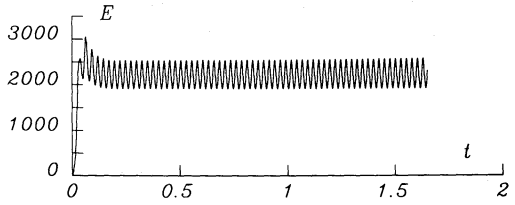

b

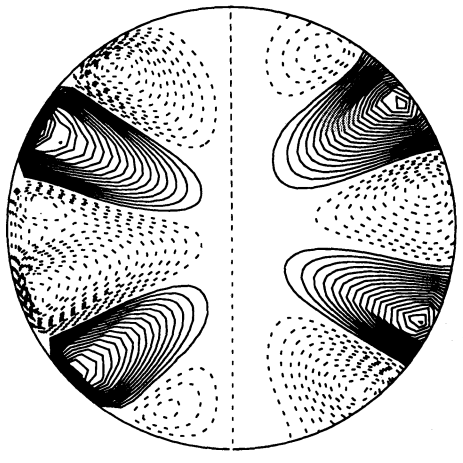

c

Fig. 4. **a** $P(t)$ for various $P(0)$, $C_\alpha = 2.0$, $\gamma = 0.01$, $C_\omega = -10^4$. **b** $E(t)$ for $P(0) = -0.9$. **c** Field configuration, $P(0) = -0.9$, $t = 1.65$

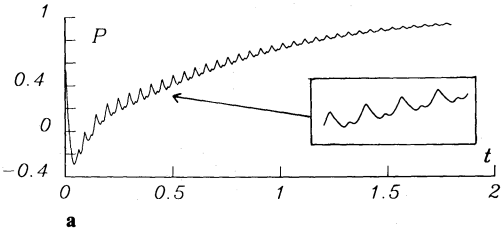

a

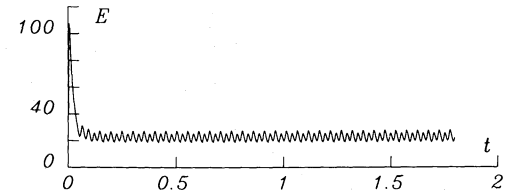

b

Fig. 5. **a** $P(t)$ and **b** $E(t)$ for $C_\alpha = 2.0$, $C_\omega = -10^4$, $\gamma = 1.0$. The inset in **a** shows details of the P-cycle for small t

amplitude, were still present. The E oscillations persisted unaltered, even when P was changing quite markedly. A quite general property of the solutions in the range of values of C_α investigated (for the given C_ω and initial field/value of γ), seems to be that a large value of $\gamma (\gtrsim 0.1)$ gives results qualitatively similar to those shown in Fig. 5, whereas a smaller value gives results more like those of Fig. 4. In fact, even when $\gamma = 0.01$, a small difference between alternate peaks of E is present, but it is not large enough to be discernable from the figures.

4.2.3. Effects of varying C_α

We now turned our attention to the effects of changing C_α with fixed initial conditions. Increasing C_α with $P(0) = 0.0$ produced qualitatively similar results to those just described when $P(0) = 0.0$ and $C_\alpha = 2$, except that the time taken to reach a state with $P \approx 1.0$ with $\gamma = 1.0$ decreased sharply with increasing C_α in the range $2 \leqslant C_\alpha \leqslant 10$, whereas when $\gamma = 0.01$ the convergence of P to $+1$ became much slower for larger values of C_α. $C_\alpha = 10.0$ was felt to be about the limit of the resolution of the code, even on a 41 $\times$ 81 grid, with these parameters and the field contours were then very concentrated towards the surface of the sphere. Approximate values of the times between the initial state with $P(0) = 0.0$ and $\langle P \rangle = 0.9$ in the range $1.2 \leqslant C_\alpha \leqslant 10.0$ are given in Table I.

We then concentrated our attention mostly on values of C_α between 2.0 and $C_\alpha^{(A)} \approx 0.54$. We first took $P(0) = 0.0$, $\gamma = 0.01$ and established that, for $C_\alpha \geqslant C_{\alpha 1} \approx 1.08$, $P \to +1$, and that for $C_\alpha \leqslant C_{\alpha 1}$, $P \to -1.0$. (A similar behaviour was noted in Paper I for pure α-quenching). The alternate maxima of E differ from one another by less than 1% (similarly the minima) and for $C_\alpha < 2.0$, P was approximately sinusoidal. By fine tuning it appears possible to locate the value $C_{\alpha 1}$ such that $\langle P(\tau) \rangle$ remains constant to an arbitrary degree of accuracy. (Here and subsequently we use $\langle f(\tau) \rangle$ to denote the mean value of f over a cycle.) Choosing $\gamma = 1.0$ gave quantitatively similar behaviour, with $1.10 < C_{\alpha 2} < 1.12$, where again $P \to +1$ for $C_\alpha > C_{\alpha 2}$ and $P \to -1$ for smaller values when $P(0) = 0.0$. (This means that there is a small range of parameter space where the value of γ, or equivalently the initial energy, determines the final parity, at least when

$P(0)=0.0$.) Now the alternate maxima and minima of E differ by much more and P is far from sinusoidal (cf., e.g., Fig. 5a) although, for $C_\alpha \gtrsim 4.0$, $P \to +1$ so rapidly that little structure is visible in $P(\tau)$. As is apparent from Table 1, as C_α approaches $C_{\alpha 1,2}$ the time to evolve to a nearly pure parity state increases sharply. Figure 12 summarizes some of these results.

We investigated the case $C_\alpha = 1.1$, $\gamma = 1.0$, at some length. The gross behaviour is displayed in Fig. 6a. However an enlargement of the interval where $\langle P(\tau) \rangle$ is changing rapidly, and also where it appears approximately constant with value near -1.0, reveals more intricate behaviour, see Fig. 6b and 6c. The modulation of the large and small oscillations (at very small amplitude) is intriguing. This modulation persisted when part of the calculation displaying this behaviour was repeated at higher resolution, but the rates of change of the envelopes were then somewhat less. We thus cannot unequivocally claim that the phenomenon will persist at still higher resolution.

4.2.4. Variation of period

We investigated the variation of cycle period (P_{cyc}) with γ at $C_\alpha = 1.10$, 2.0 and 6.0, but found negligible difference between the periods of the solutions for $\gamma = 0.0$, and 1.0 (defined by the interval between alternate peaks in the energy curves). The variation of P_{cyc} with C_α is given in Table 2. For $C_\alpha \gtrsim 1.0$ the relation $P_{cyc} \propto C_\alpha^{-0.5}$ is valid.

4.2.5. Trends with changing C_ω

We made a limited study of the effects of changing the angular velocity gradient, C_ω. In the purely buoyancy limited case at constant C_α, for strictly odd parity solutions the mean value of E in the oscillatory steady state was approximately proportional to $|C_\omega|$ – see Table 3 (here and elsewhere all logarithms are to base 10). These solutions are unstable to even parity perturbations (see above), but we feel that this is irrelevant to this discussion. Approximately the same relation was obtained for pure α-quenching (Table 3 also). This is perhaps not altogether surprising, as in each case the feedback depends on $\mathbf{B}^2$, and the equilibration condition is of the form $\mathbf{B}^2 \propto |C_\omega|$. We also investigated models with $\gamma \sim |\mathbf{B}|$ (see Sects. 4.4 and 4.5). In these cases $|\mathbf{B}| \sim |C_\omega|$ and so $E \propto C_\omega^2$. We note also that a dynamo model limited dynamically by the action of the Lorentz forces shows a similar dependence of E – see Fig. 1 of Paper II. For both the buoyancy limited and α-quenched models the frequency increases as $|C_\omega|^{(0.5-0.6)}$, with a slightly steeper dependence in the buoyancy-limited case.

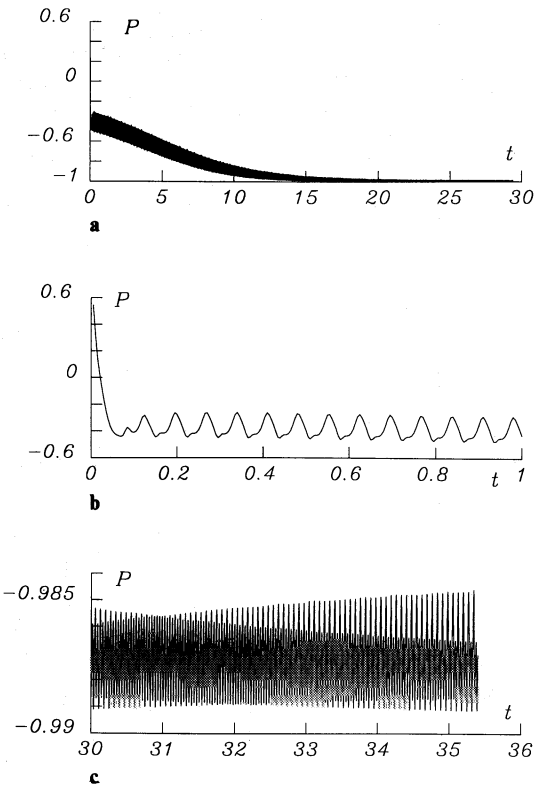

Fig. 6a–c. $C_\alpha = 1.1$, $\gamma = 0.01$, $C_\omega = -10^4$. **a** Gross structure of P. **b** Pulse structure for small t. **c** Modulation of pulse at large t

Table 2. Variation of cycle period with C_α for buoyancy limited models. $C_\omega = -10^4$, $\alpha_B = 0.0$, $\gamma = 1.0$

C_α	P_{cyc}	P
0.55	0.116	−1.0
0.7	0.098	−1.0
1.1	0.070	mixed soln
2.0	0.050	1.0
6.0	0.029	1.0
10.0	0.023	1.0

Table 1. Time τ taken between initial state with $P(0)=0.0$ and $\langle P(t) \rangle \simeq 0.9$ for $\alpha^2\omega$ dynamo, $\alpha_B = 0$

C_α	$\gamma = 0.01$	$\gamma = 1.0$
0.7	0.35	
1.0	3.0	
1.2	2.3	4.5
1.5	0.65	
2.0	0.16	1.6
4.0	0.8	
6.0	1.65	0.10
10.0	$\gtrsim 3.0$	0.065

4.3. $\alpha^2\omega$ dynamo with buoyancy and α-quenching

We now allowed two types of nonlinearity to operate simultaneously – buoyancy and α-quenching, the latter modelled by Eq. (2.7). Now the equations cannot be scaled to a single value of γ or α_B (even given consistent initial conditions) and the relative sizes of α_B and γ are important, even for identical initial field configurations.

Table 3. $C_\alpha = 10$. The dependence of the mean magnetic energy on C_ω for odd parity solutions. The amplitude of the oscillation about the mean is also given. ω is the frequency and Q is the ratio of poloidal to toroidal energy. The normalization of the energies for the α-quenched and buoyancy limited cases is different. (The small difference in the frequency for the buoyancy limited model with $C_\omega = -10^4$ compared with that of Table 2 is attributable to the different spatial resolution)

Buoyancy limited, $\gamma \propto \mathbf{B}^2$				α-quenched		
C_ω	log E	Q	ω	log E	Q	ω
-10^3	0.95 ± 0.1	0.07 ± 0.02	79	-0.20 ± 0.15	0.05 ± 0.015	63
-3×10^3	1.52 ± 0.04	0.04 ± 0.003	157	0.40 ± 0.1	0.012 ± 0.003	99
-10^4	2.0 ± 0.03	0.05 ± 0.02	250	0.73 ± 0.1	0.003 ± 0.0003	173
-3×10^4	2.4 ± 0.2	0.05 ± 0.03	600			
Buoyancy limited, $\gamma \propto \lvert\mathbf{B}\rvert$				Buoyancy limited, $\gamma \propto \lvert\mathbf{B}_T\rvert$		
C_ω	log E	Q	ω	log E	Q	ω
-10^3	1.85 ± 0.11	0.075	80	1.91 ± 0.11	0.075	80
-3×10^3	2.86 ± 0.05	0.032	180	2.90 ± 0.05	0.031	180
-10^4	3.73 ± 0.02	0.011	280	3.75 ± 0.02	0.011	280

4.3.1. Influence of initial parity

After some experimentation we decided to investigate the effects of changing the parity of the initial state for parameter values $\gamma = 1.0$, $\alpha_B = 0.1$, $C_\alpha = 1.2$ (and, as always, $C_\omega = -10^4$). $P(\tau)$ is displayed in Fig. 7a for several values of $P(0)$. Although for $P(0) \neq -1.0$ we always found that $P \to +1.0$, the detailed behaviour of the solutions as a function of $P(0)$ is quite complex. The most obvious feature is the rate of change of P. When $P(0) = 0.9$ then $P \approx +1.0$ for $\tau \geqslant 0.2$ whereas with $P(0) = -0.9$ a time $\tau > 3$ is needed. For $P(0) \lesssim 0.5$ P displays a complex oscillatory behaviour. Even when, at the resolution of Fig. 7a, P appears to be constant, a "blow up" shows that P continues to vary. The pulse shapes for $P(0) = \pm 0.9$ are given in Fig. 7b: that for $P(0) = +0.9$ is constant in form by $\tau = 2$, whilst that for $P(0) = -0.9$ is still slowly changing in amplitude at $\tau = 5.0$, although the basic pulse shape seems to be constant.

However it is the behaviour of the energy, E, that is more distinctive. For all $P(0) > 0.0$ the final oscillatory state is the same. There is then a marked difference between alternate peaks. For $P(0) \leqslant 0.0$ the final state gradually changes, so that by $P(0) = -1.0$ the difference between peaks is considerably reduced. Details of the variation of E for $P(0) = 0.9$ when $\langle E(\tau) \rangle$ is eventually constant are given in Fig. 7c and the solutions are summarized in Table 4 (where superscripts (1) and (2) refer to the "large" and "small" maxima and minima).

4.3.2. The cycle periods

The cycle periods when $C_\alpha = 1.2$, $C_\omega = -10^4$ are given in Table 5 for a selection of values of α_B and γ. Note that at constant α_B, the cycle period decreases with increasing buoyancy parameter γ.

4.3.3. Transition between buoyancy and α-quenching dominated behaviour

For $C_\alpha = 1.2$ the transition in behaviour between pure α-quenching and buoyancy dominated behaviour at $\alpha_B = 0.01$ and $P(0)$

Table 4. Results for $C_\alpha = 1.2$, $C_\omega = -10^{-4}$, $\gamma = 0.01$, $\alpha_B = 0.1$, parity of initial field configuration varying. (1) and (2) refer to the alternate peaks, c.f. Fig. 7c

$P(0)$	log $E_{max}(1)$	log $E_{max}(2)$	log $E_{min}(1)$	log $E_{min}(2)$
0.9	0.971	0.880	0.674	0.620
0.1	0.971	0.880	0.674	0.620
0.0	0.970	0.879	0.676	0.619
−0.1	0.967	0.883	0.673	0.623
−0.5	0.953	0.890	0.667	0.633
−0.9	0.937	0.916	0.653	0.641
−1.0	0.907	0.904	0.693	0.700

Table 5. Variation of periods, $C_\alpha = 1.2$, $C_\omega = -10^4$

α_B	γ	P_{cyc}
0.00	0.01	0.067
0.01	0.0	0.088
	0.01	0.087
	1.0	0.070
	4.0	0.068
1.0	0.0	0.086
	0.01	0.086
	1.0	0.085

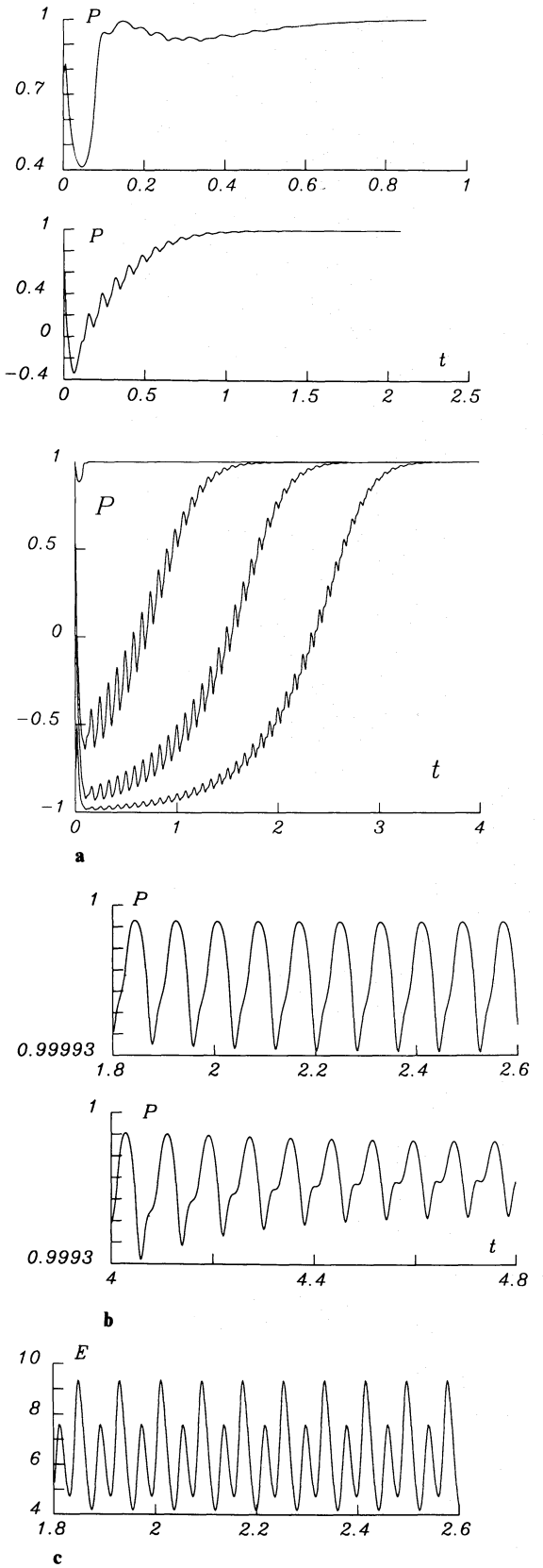

Fig. 7. **a** $P(t)$ for $P(0)=0.9, 0.0, -0.5, -0.9$ (main panel) and $P(0)=0.5$, 0.1 (small panel) for $C_\alpha=1.2$, $\alpha_B=0.1$, $\gamma=1.0$, $C_\omega=-10^4$. **b** Details of pulse shapes for large t when $P(0)=+0.9$ (upper) and -0.9 (lower). **c** $E(t)$ for $P(0)=0.9$

Table 6. Dependence of the mean magnetic energy on γ for a model with α-quenching also present $C_\alpha=1.2$, $\alpha_B=0.01$, $C_\omega=-10^4$

γ	$\langle \log E \rangle$
0.000	97.2
0.001	97.2
0.01	97.1
1.0	11.5
4.0	3.0

$=0.0$ was investigated. Figures 8a–d display $E(\tau)$ and $P(\tau)$ for $\gamma=0.001$, 0.01, 1.0 and 4.0 ($\gamma=0.0$ was very similar to $\gamma=0.001$). Table 6 gives the mean values of E in the final states. The last two entries are clearly in the "γ-dominated" regime, where $E \propto \gamma^{-1}$.

A similar investigation was carried out for the same value of C_α and $\gamma=0.01$ with $0.0 \leqslant \alpha_B \leqslant 1.0$. With $\alpha_B=1.0$ a limit cycle with $0.985 \lesssim P \lesssim 1.0$ was rapidly established, see Fig. 9a. This was very similar to the result with $\gamma=0.0$. Figure 9b also displays the variation of E and the ratio of poloidal to toroidal energy for this case. In contrast, for smaller values of α_B, the limit cycle behaviour vanishes but now the oscillation in E displays larger and smaller maxima and minima, see Fig. 9c for $\alpha_B=0.1$ (where the limit cycle is present but smaller in amplitude than in Fig. 9a) and for $\alpha_B=0.01$. For still smaller (and zero) values of α_B this "double wave" behaviour of E is not seen, as the maxima become of equal size. The asymmetric form of E_p/E_t (Fig. 9b) (essentially due to E_p) also disappears as α_B becomes smaller.

$C_\alpha=1.2$ is above the critical values $C_{\alpha 1,2}$ which mark the watershed for the purely buoyancy-limited dynamo between ultimate even and odd parity states (at $P(0)=0.0$ at least). Thus we performed similar computations to the above for $\gamma=1.0$, $C_\alpha=1.1$ and 1.05 (both values less than $C_{\alpha 2}$). For $C_\alpha=1.1$ we deduced that $\alpha_B \approx 0.01$ resulted in a stable limit cycle solution which could be thought of as a balance between the conflicting influences of buoyancy and α-quenching. For $C_\alpha=1.05$, $\gamma=1.0$ we similarly found a value α_{B1}, $0.01<\alpha_{B1}<0.10$, such that for $\alpha_B>\alpha_{B1}$ $P\to+1$ (as in the purely α-quenched solutions) and for $\alpha<\alpha_{B1}$ $P\to-1$, as in the purely buoyancy-limited solutions.

4.3.4. Effects of buoyancy on "torus" and "limit cycle" solutions of Papers I and II

Experiments with pure α-quenching (Papers I and II) discovered solutions in a limited range of C_α ($0.8 \lesssim C_\alpha \lesssim 0.9$) whose phase space trajectories were tori, in addition to limit cycle solutions that were sometimes of mixed parity. Whilst we certainly cannot claim that we have explored all the parameter space available for purely buoyancy-limited dynamos (C_α value, γ/initial conditions) we were not able to discover torus-type solutions in this model. Moreover our experiments with simultaneous buoyancy and α-quenching for values of C_α larger than this range, described above, only found unchanging limit cycles of small amplitude in P, except for very special cases. We therefore decided to investigate how a pure α-quenching torus solution was affected by the inclusion of buoyancy. We took as our starting point the solution

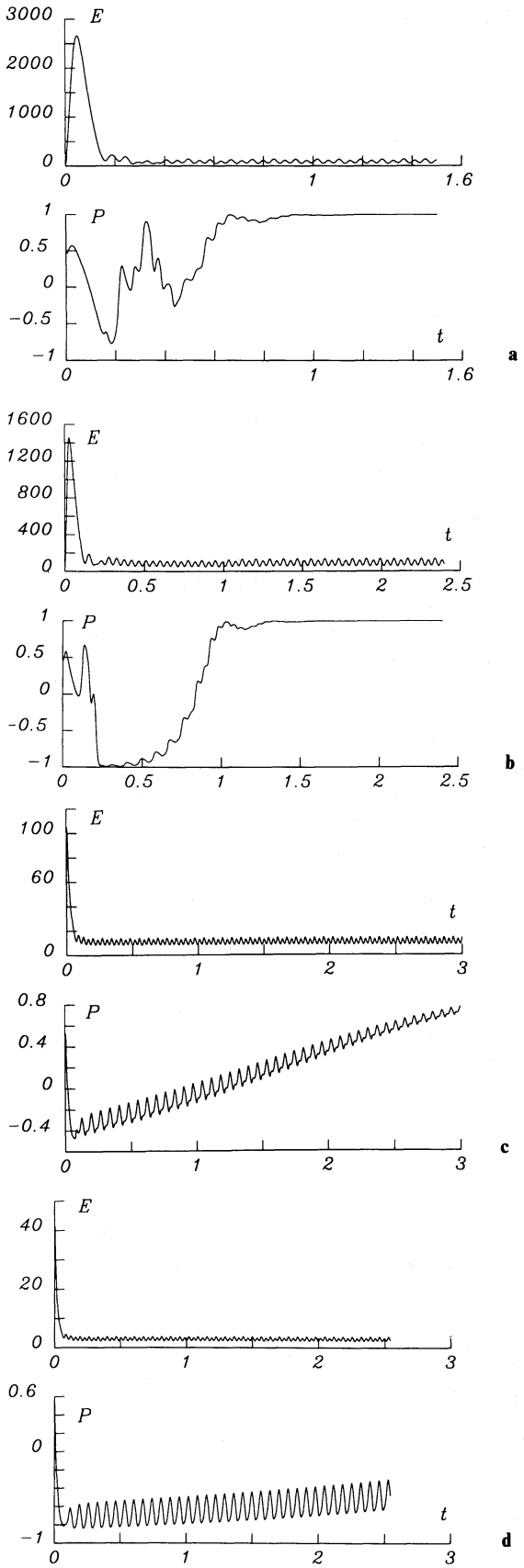

Fig. 8a–d. $E(t)$, $P(t)$ for $\alpha_B=0.01$, $C_\alpha=1.2$, $C_\omega=-10^4$. **a** $\gamma=0.0001$. **b** $\gamma=0.01$. **c** $\gamma=1.0$. (P approaches $+1$ closely by $t=5$). **d** $\gamma=4.0$

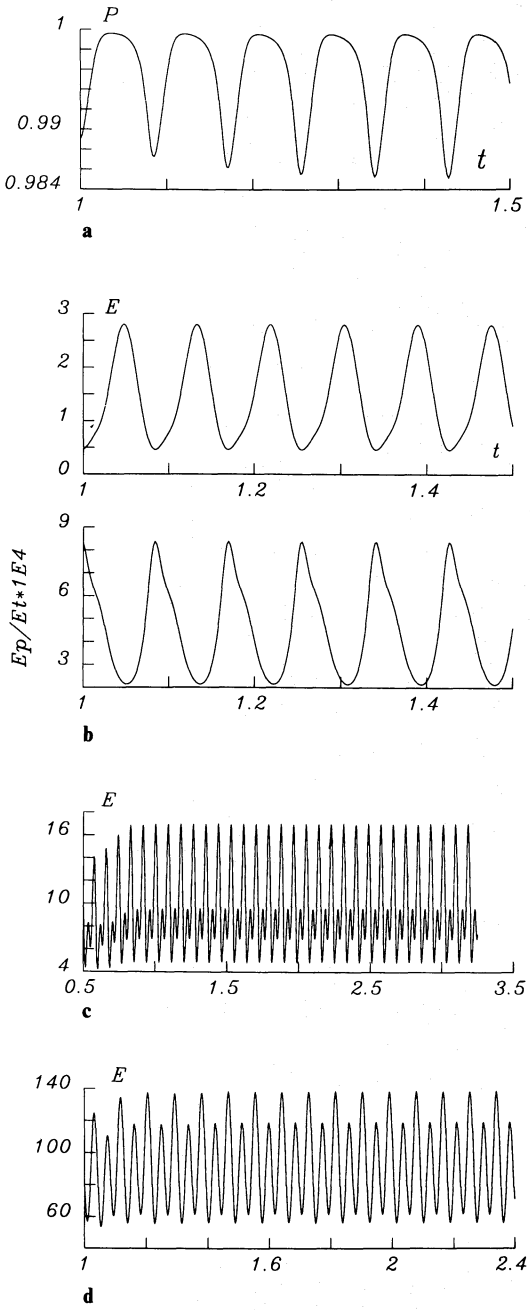

Fig. 9a–d. $\gamma=0.01$, $C_\alpha=1.2$, $C_\omega=-10^4$. **a** $P(t)$ for $\alpha_B=1.0$. **b** $E(t)$, E_p/E_t for $\alpha_B=1.0$.**c** $E(t)$ for $\alpha_B=0.1$. **d** $E(t)$ for $\alpha_B=0.01$

with $C_\alpha=0.9$, $\alpha_B=1.0$, $\gamma=0.0$. The solution discussed in Paper I requires a 41×81 grid for its accurate representation. To economize on computer time we ran our computations on a 21×41 grid, which satisfactorily reproduced the main features of the more accurate calculations but gave, for example, a somewhat different modulation of $P(\tau)$. This $\gamma=0.0$ solution is displayed in Fig. 10a. For values of $\gamma\leqslant1.0$ this solution was little altered. When $\gamma=10.0$ the torus is effectively destroyed – see Fig. 10b., which shows $P(\tau)$ and $E(\tau)$ in this case. The period of $E(\tau)$, determined from the major maxima of Fig. 10a and b, decreases by 3 or 4% when $\gamma=10.0$ as compared to $\gamma=0.0$. Similarly we studied the effects of buoyancy on a large amplitude limit cycle

solution of the type investigated in Paper I. With $C_\alpha = 0.8$, $\alpha_B = 1.0$ and $\gamma = 0.01$ the solution was little changed from that with $\gamma = 0.0$ (Fig. 11a). As γ increased from 1.0 to 10.0, $P(\tau)$ decreased. The amplitude of its cycle was markedly reduced and the form altered somewhat, see Fig. 11b. The period of the oscillation of E decreased by about 10% from $\gamma = 0.0$ to 10.0.

4.4. *Buoyant rise velocity proportional to v_A*

We reinvestigated three illustrative cases taking u_B of the form (8). For an α^2 dynamo with $C_\alpha = 10.0$ we found behaviour very similar to that described in Sect. 4.1. In particular there was again a watershed between $P(0) = 0.0$ and 0.1 separating solutions with $P \to -1.0$ and $+1.0$, and the ratio of poloidal to toroidal energies in the final stage were very little altered. Only a small difference in field contours was apparent. We also recalculated the $\alpha^2\omega$ dynamo with $C_\alpha = 1.0$ and 2.0 (cf. Sect. 4.2.1). As before we found that when $C_\alpha = 1.0$ the eventual state was $P = -1.0$ and when $C_\alpha = 2.0$ $P \to +1.0$ always. Ratios of poloidal to toroidal energy were quite similar to those of the earlier calculations and the detailed behaviour of the solution was remarkably little changed.

The only distinctive alteration to our results caused by changing the functional form of γ is seen when we examine the dependence of the energy on C_ω. Now $\langle E \rangle \propto C_\omega^2$ – see Table 3.

4.5. *Buoyant rise velocity proportional to $|B_T|$*

Because the toroidal field is dominant in our $\alpha^2\omega$ dynamo calculations we calculated only α^2 models with $C_\alpha = 10.0$ to check the effect of taking $|u_B| \propto |\mathbf{B}_T|$. As before (Sects. 4.2.1 and 4.4) we found that $P(0) \geqslant 0.1$ gave $P \to +1.0$ and $P(0) \leqslant 0.0$ gave $P \to -1.0$. The ratios of poloidal to toroidal energy and the field contours were quite similar to those of the other models with $C_\alpha = 10.0$. Again $\langle E \rangle \propto C_\omega^2$, Table 3.

5. Discussion

A somewhat surprising result is the absence of strong, stable, 'mixed-mode' solutions, in contrast both to the results of Paper II for α-quenched dynamos and to recent results of Jennings and Weiss (preprint) for 1 dimensional buoyancy-limited dynamos. The latter work reports a large variety of bifurcation phenomena. We speculate that we might find a larger range of behaviour in a spherical shell geometry, especially if we simulated a dynamo seated in a relatively thin layer at the base of the convective layer. This belief is partly based on the physical argument that buoyancy could then more effectively remove field from the dynamo region, but also on the relationship between a thin shell dynamo and 1 dimensional dynamos (e.g. Jennings, Brandenburg, Moss and Tuominen, 1990).

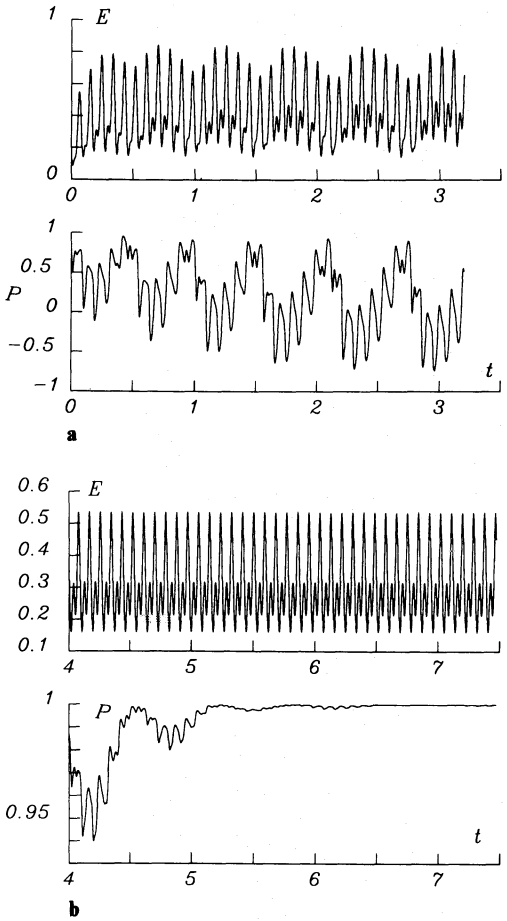

Fig. 10. **a** $C_\alpha = 0.9$, $\alpha_B = 1.0$, $C_\omega = -10^4$, $\gamma = 0.0$, torus solution. **b** Continuation of solution shown in 10a) with $\gamma = 10.0$

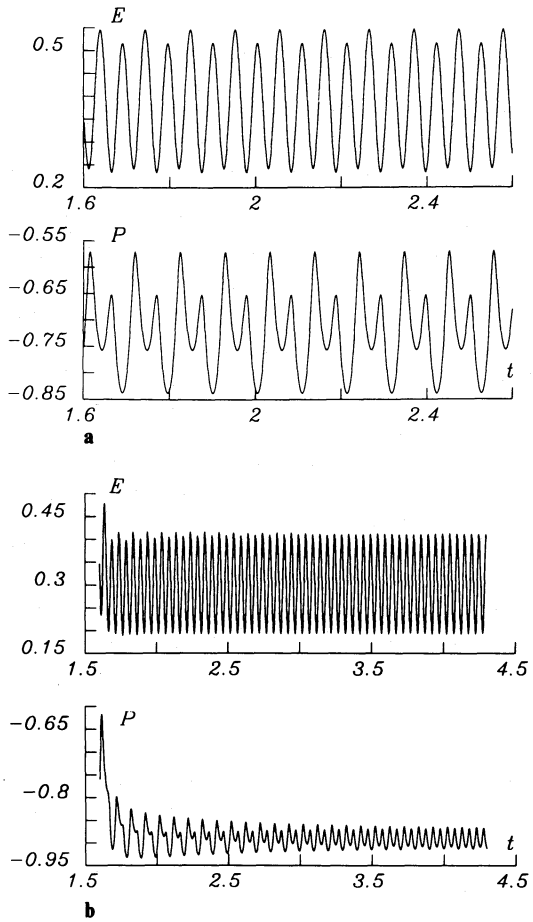

Fig. 11. **a** $C_\alpha = 0.8$, $\alpha_B = 1.0$, $C_\omega = -10^4$, $\gamma = 0.01$, limit cycle. **b** Solution with same C_α, α_B as 11a), but $\gamma = 10.0$, started from limit cycle solution at $t = 1.6$

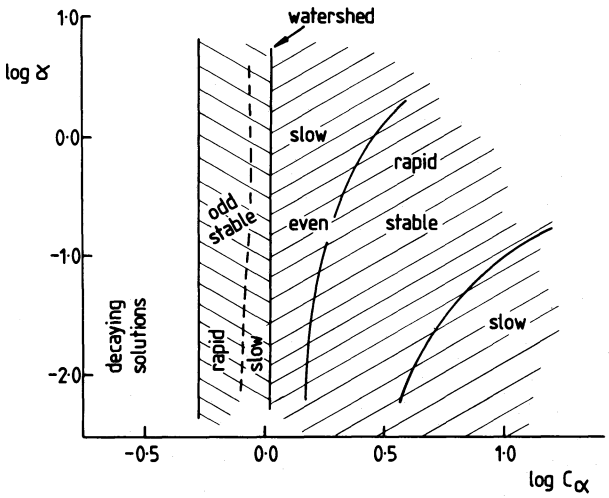

Fig. 12. Summary of $\alpha^2\omega$ calculations with $\alpha_B=0$, $C_\omega=-10^4$. "SLOW" and "RAPID" refer to the rate of adjustment towards $P=\pm 1.0$. The borders are drawn, very approximately where, for $P(0)=0.0$, the time $t(0.9)$ for P to attain the value ± 0.9, is approximately unity. The line marked "WATERSHED" separates (for $P(0)=0.0$ at least) the regions where even and odd parity solutions are stable. There $t(0.9)\to\infty$. Numerical experiments described in the text indicate that the position of the watershed depends little, if at all, on the value of the initial parity $P(0)$

Turning to our more detailed results the main inferences and conclusions are as follows.

1. The analytical form of the term representing the effects of buoyancy is not critical. The results presented in Sects. 4.4 and 4.5 do not differ significantly from those in the bulk of this paper.

2. In the purely buoyancy-limited α^2 dynamo there may be two stable solutions, of odd and even parity, when $C_\alpha > C_\alpha^{(S)}$. The existence of this property depends on the magnitude of C_α. Solutions for the α^2 dynamo do not seem to depend on the value of γ, equivalently the initial field energy, for a given $P(0)$.

3. In the purely buoyancy limited $\alpha^2\omega$ dynamo, odd parity solutions are stable when $C_\alpha < C_{\alpha\text{crit}}$ and purely or almost purely even parity solutions are stable with $C_\alpha > C_{\alpha\text{crit}}$ (see Fig. 12). Now the form of the oscillations in the total energy depends on the magnitude of γ. Larger values of γ tend to give asymmetric cycles with alternate peaks in E of different sizes.

4. In the purely buoyancy limited dynamo, except very near to $C_{\alpha 1,2}$ (see Sect. 4.2.3), the eventual oscillations in P (if present) are of very small amplitude, although typically quite non-sinusoidal in form. No torus type solutions were found, and limit cycle solutions with large amplitude in P exist only for very carefully tuned parameter values.

5. When both buoyancy and a nonlinear α-effect (depending on the local magnetic energy density) operate, increasing the value of γ eventually destroys the tori solutions and much reduces the amplitude of the oscillations in P in the large amplitude limit cycle solutions that were described in Paper II.

6. The effect of buoyancy on the periods of our solutions is small. Increasing the size of γ shortens the periods slightly.

7. The dependence of magnetic activity on stellar rotation is of fundamental importance. Our models are, as yet, far too idealized to throw any real light on the matter. For what it is worth we note that our work predicts an increase in cycle frequency with radial angular velocity gradient ($\omega \propto |C_\omega|^{0.5}$).

The second and third of these conclusions are similar to those of Paper II concerning nonlinear α-limited dynamos. We note with interest the asymmetry in energy between successive half cycles. Whilst too regular to be of immediate interest to the solar cycle this effect could be significant in a more sophisticated model.

Finally we reiterate some of the more glaring limitations of our work. It can only be an exploratory, highly parameterized, investigation of the grosser effects of buoyancy. Of course, the model can be elaborated, although it is doubtful that much effort in this direction is justifiable without a better understanding of the dynamics of magnetic convection zones. We have limited our calculations to a complete sphere, rather than a spherical shell, largely to facilitate comparison with our earlier work. True dynamics are absent – although in principle we could include this, or a similar, parameterization of buoyancy in a dynamical calculation, cf. Paper I. Our computations explore only a fragment of parameter space. Parts are inaccessible because higher resolution than we can achieve is needed but, in any case, the computational resources needed for a thorough exploration are enormous. Quite possibly we have overlooked regions of interest. And, of course, our computations are limited to strict axisymmetry. We repeat the caveat given in Paper II – some of our apparently stable solutions may be unstable to non-axisymmetric perturbations. Rädler and Wiedemann (1989) have produced some limited evidence that this may be the case, although they have not determined what the eventual stable solution would then be (see also Jennings et al., 1990).

References

Brandenburg, A., Krause, F., Meinel, R., Moss, D., Tuominen, I.: 1989a, *Astron. Astrophys.* **213**, 411 (Paper I)

Brandenburg, A., Moss, D. Tuominen, I.: 1989b, *Geophys. Astrophys. Fluid. Dyn.* (in press) (Paper II)

Brandenburg, A., Tuominen, I.: 1988, *Adv. Space Res.* **8** (7), 185

Jennings, R., Brandenburg, A., Moss, D., Tuominen, I.: 1990, *Astron. Astrophys.* (in press)

Krause, F., Meinel, R.: 1988, *Geophys. Astrophys. Fluid. Dyn.* **43**, 95

Jones, C.A., Weiss, N.O., Cattaneo, F.: 1985, *Physica* **14D**, 161

Lorenz, E.N.: 1963, *J. Atmosph. Sci.* **20**, 130; **20**, 448

Moreno-Insertis, F.: 1983, *Astron. Astrophys.* **122**, 241

Moss, D., Tuominen, I.: 1989, *Geophys. Astrophys. Fluid. Dyn.* (in press)

Noyes, R.W., Weiss, N.O., Vaughan, A.H.: 1984, *Astrophys. J.* **287**, 769

Parker, E.N.: 1979, *Cosmical Magnetic Fields*, Clarendon Press, Oxford

Rädler, K.H., Wiedemann, E.: 1989, *Geophys. Astrophys. Fluid. Dyn.* (in press)

Roberts, P.H.: 1972, *Phil. Trans. Roy. Soc. A* **272**, 663

Ruzmaikin, A.A.: 1981, *Comments on Astrophysics* **9**, 85

Steenbeck, M., Krause, F.: 1969, *Astron. Nachr.* **291**, 49

Van Ballegooijen, A.A.: 1982, *Astron. Astrophys.* **133**, 99